iScience

Article

MHC2-SCALE enhances identification of immunogenic neoantigens

Graphical abstract

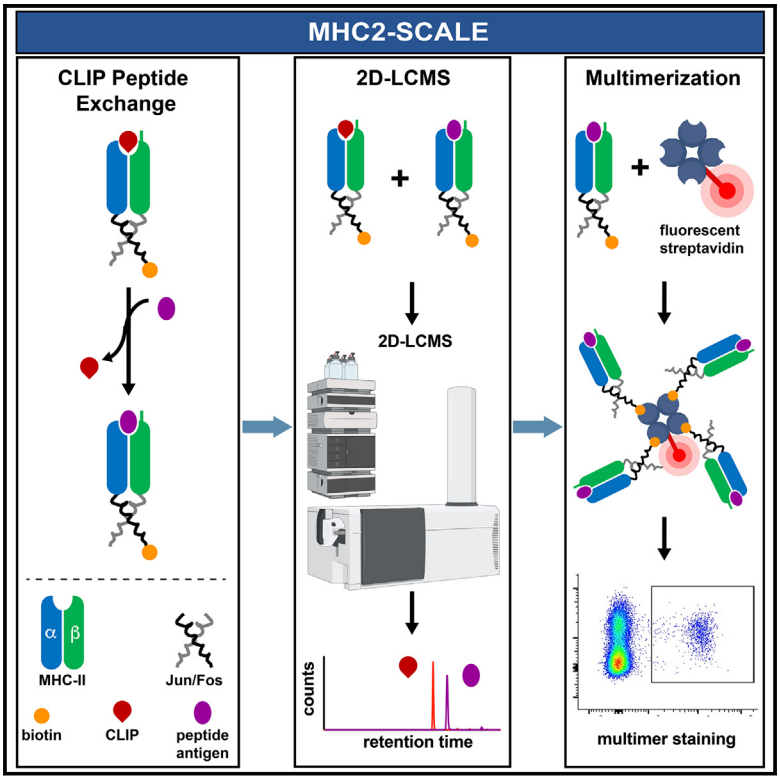

Highlights

- MHC2-SCALE workflow was developed and optimized
- This process enables sensitive and accurate detection of MHC2 epitopes
- MHC2-SCALE is compatible with a broad range of peptide epitopes and MHC2 alleles
- MHC2-SCALE identifies true binders not predicted by IEDB algorithms

Authors

Joshua G. Gober, Aude-Hélène Capietto, Reyhane Hoshyar, ..., Jonathan L. Linehan, Lélia Delamarre, Adel M. ElSohly

Correspondence

elsohly.adel@gene.com

In brief

Biological sciences; Biochemistry methods; Immunology; Proteomics

Gober et al., 2025, iScience *28*, 112212
April 18, 2025
https://doi.org/10.1016/j.isci.2025.112212

CellPress

iScience

CellPress
OPEN ACCESS

Article

MHC2-SCALE enhances identification of immunogenic neoantigens

Joshua G. Gober,[1,4] Aude-Hélène Capietto,[2,4] Reyhane Hoshyar,[2] Martine Darwish,[1] Richard Vandlen,[1] Jonathan L. Linehan,[2] Lélia Delamarre,[2] and Adel M. ElSohly[1,3,5,*]

[1]Department of Protein Chemistry, Genentech Inc, South San Francisco, CA, USA
[2]Cancer Immunology Department, Genentech Inc, South San Francisco, CA, USA
[3]Department of Immunology Discovery, Genentech Inc, South San Francisco, CA, USA
[4]These authors contributed equally
[5]Lead contact
*Correspondence: elsohly.adel@gene.com
https://doi.org/10.1016/j.isci.2025.112212

SUMMARY

Recent studies suggest that CD4$^+$ T cells can exert potent anti-tumor effects and improve immunotherapy efficacy by aiding CD8$^+$ T cells. However, characterizing the mechanism of CD4$^+$ T cells' anti-tumor activity has been challenging due to inaccurate major histocompatibility complex class II (MHC-II) peptide prediction algorithms and the lack of high-quality reagents for immune monitoring. To address this, we developed MHC2—substitution of CLIP and analytical LCMS evaluation (MHC2-SCALE), a streamlined approach combining affinity optimized class II-associated invariant chain peptide (CLIP) exchange technology, high throughput 2D-LCMS analysis, and rapid generation of peptide-bound MHC-II monomers for subsequent multimer assembly. We validated MHC-II peptide candidates predicted by the immune epitope database (IEDB) algorithm, as well as uncovered many true and immunogenic MHC-II binders that were not predicted by IEDB. Thus, MHC2-SCALE expands the opportunities for discovering, tracking, and phenotyping antigen-specific CD4$^+$ T cells in preclinical and clinical settings, thereby improving therapies for cancer, autoimmunity, or infectious diseases.

INTRODUCTION

CD4$^+$ T cells are a pivotal component of the immune system that play diverse and crucial roles in adaptive immunity. CD4$^+$ T cells include two major subsets, T effector cells (also called helper T (Th) cells or T follicular helper (Tfh) cells) and T-regulatory cells (Tregs) with opposite functions. Effector CD4$^+$ T cells participate in the activation of cell-mediated immunity by supporting the functional maturation of cytotoxic CD8$^+$ T cells, promoting and modulating humoral immunity through aiding B cells in antibody class switching, and directly exerting cytotoxic effects against abnormal or infected cells. Conversely, Tregs operate on the opposite end of the spectrum and exhibit immunosuppressive functions that help maintain self-tolerance but also lead to disease progression.[1] In the case of malignant tumors, the presence, density, and functional polarization of tumor-infiltrating CD4$^+$ T cells have been shown to bear prognostic significance in various cancer types,[2–8] underscoring their pivotal role in cancer biology. However, the complexity of the various subsets (Th1, Th2, Th17, Tfh, and Tregs), each with distinct functions and characteristics, makes it difficult to discern the overall effect of CD4$^+$ T cells in cancer progression. While depleting immunosuppressive Treg populations has shown some efficacy in the clinic, significant toxicity limits the use of this strategy.[9,10] More recently, it has become increasingly clear that boosting tumor-reactive CD4$^+$ T helper cells can provide effective anti-tumor responses with less severe side effects.[11–15] Thus, understanding the complex roles of the versatile subsets of tumor-specific CD4$^+$ T cells is essential for the development of effective immunotherapeutic strategies.

CD4$^+$ T cell subpopulations can be characterized using technologies similar to those developed for CD8$^+$ T cells, such as functional assays (ELISpot), TCR sequencing, and flow cytometric analysis using fluorescently labeled major histocompatibility complex (MHC) multimers. However, the isolation of tumor-specific CD4$^+$ T cells can be difficult due to the slower rate of effector CD4$^+$ T cell proliferation relative to CD8$^+$ T cells. In addition, MHC-II molecules are more complex than MHC-I, rendering the monomer generation process and subsequent CD4$^+$ T cell multimer staining more challenging. First, MHC-II molecules are made of two chains (alpha and beta) that are both polymorphic in comparison to only one polymorphic heavy chain (alpha) for MHC-I. Additionally, the length of the peptides that bind to MHC-II have N and/or C-terminal extensions outside of the 9 amino acid (aa) binding core (10–30 aa total length) that fit in the open binding groove as opposed to MHC-I that has a closed binding groove that accommodates peptides of only 8–12 aa in length. These distinctions make the prediction of MHC-II binders more difficult and generally less accurate. Furthermore, the binding affinity of the co-receptor CD4 to MHC-II is much lower than

the affinity of co-receptor CD8 to MHC-I, rendering the avidity, and thus the T cell staining efficiency of pMHC-II multimers lower than that of pMHC-I multimers.

Traditional methods for $CD4^+$ T cell staining with MHC-II multimers have relied on monomer formation using either recombinant expression of covalently linked candidate peptide epitopes to the MHC-II beta chain N terminus[16,17] or the attachment of affinity tags to peptides of interest and subsequent purification after peptide exchange.[18,19] Recombinant expression technologies can enable the low throughput preparation of monomer reagents, but for poorly expressing or lower-affinity peptides, this approach often requires extensive construct optimization to enable expression. To overcome this challenge, cysteine trapping technologies are often used to anchor the fused peptide in a particular register of the binding groove and often facilitate higher expression yields.[20] An important limitation is that peptides containing cysteine residues are incompatible with this approach. In contrast, peptide exchange technologies are more general and can be used for many peptide sequences. However, commonly used peptide exchange protocols often require two steps (affinity capture and size exclusion), which limits the number of reagents that can be assembled in a high throughput manner. As such, neither of these approaches is amenable to high throughput screening of peptide epitopes or preparation of monomers suitable for multimer assembly. Recently, approaches to generate MHC-II monomers relying on the use of HLA-DM as a catalyst were reported[21,22]; however, this method requires purification of the mixture in order to assess the extent of peptide exchange, which precludes the ability to directly perform QC on the unpurified MHC-II monomers used for multimer assembly. While the use of HLA-DM facilitates peptide exchange,[23–25] it has also been reported that HLA-DM limits the diversity of peptides that can be presented on cell surfaces in the absence of HLA-DO,[26] suggesting that only higher affinity pMHC-II complexes can be formed in this fashion.

With these limitations in mind, we developed a new approach, called MHC2-SCALE (substitution of CLIP and analytical LCMS evaluation), that combines 3 optimized protocols into a streamlined workflow to generate and characterize pMHC-II reagents: (1) affinity optimized CLIP peptide exchange, (2) two-dimensional liquid chromatography-mass spectrometry (2D-LCMS), and (3) purification-free multimerization. By optimizing affinity attenuated class II-associated invariant chain peptides (CLIPs) for mouse and human alleles, we enable peptide exchange and simplify the overall monomer generation process. The 2D-LCMS step enables high-resolution mass characterization of individual components from complex samples, thus allowing discrimination between impurities and peptides of interest, serving as a critical QC step to enable reproducible reagent preparation and determine when complete peptide exchange has occurred. The *in situ* QC by 2D-LCMS enables a facile multimerization protocol without the need for monomer purification. We demonstrate the utility of MHC2-SCALE for discovering and screening MHC-II binding epitopes of murine and human alleles as well as staining of $CD4^+$ T cells, providing a new high-throughput approach for monitoring and characterizing these cells in preclinical and clinical settings.

Design

Current methods for identifying and monitoring antigen-specific CD4 T cells are often labor-intensive and limited in their ability to accommodate a wide range of peptide sequences. Additionally, these techniques can yield inaccurate results due to potential impurities in the samples. The MH2-SCALE approach overcomes these challenges by integrating a high-throughput peptide exchange technique using affinity-optimized class II-associated invariant chain peptide (CLIP) variants, a 2D-LCMS method for detailed analysis of the peptide exchange process, and a rapid system for generating peptide-bound MHC-II monomers for multimer assembly. This combined approach enables: (1) the effective identification of peptides that bind to MHC-II molecules, (2) the efficient production of peptide-bound MHC-II monomers, and (3) the rapid, purification-free multimerization with fluorophores for specific cell detection, such as through flow cytometry. The 2D-LCMS method further provides a robust, label-free quality control system, ensuring precise reagent characterization and protocol optimization for peptide exchange, including for cysteine-containing peptides.

RESULTS

Peptide exchange and 2D-LCMS optimization

To develop MHC2-SCALE, we first optimized the construct design and expression system of the MHC-II proteins. The most commonly used recombinant platforms for MHC-II proteins are insect or mammalian cell expression of alpha and beta chains fused to coiled-coil or leucine zipper heterodimerization motifs on the C termini.[17,18,20,27–31] The antigenic peptide of interest or the CLIP peptide is almost invariably fused to the N terminus of the beta chain,[16,17] and several reports have indicated that the level of expression of the assembled heterodimer is highly dependent on the affinity of this peptide for the MHC-II allele. We optimized these types of constructs with the mouse MHC-II $I\text{-}A^b$ allele using the murine CLIP peptide (mCLIP) fused to a flexible Gly-Ser linker containing a TEV cleavage site to enable high-yield expression (>100 mg/L after 2-column purifications) in CHO cells and provide ample protein for further optimization efforts (summarized in Figure 1A).

Next, we used mCLIP-$I\text{-}A^b$ to develop a 2D-LCMS protocol that built upon our previous experience with MHC-I alleles.[32–34] Briefly, the instrument setup relies on a first-dimension size exclusion column run under native conditions to isolate the intact complex in a separate loop from any unbound peptides. The isolated complex is then injected directly onto a reversed-phase HPLC column and subjected to electrospray ionization (Figure 1B). Importantly, this protocol allows for direct analysis of the bound peptides in the complex. To validate this method, the TEV linker in the mCLIP-$I\text{-}A^b$ complex was cleaved and analyzed by 2D-LCMS. Clear size exclusion chromatography (SEC) isolation of the complex was achieved, and the mCLIP peptide was readily detected.

For proof of concept, peptide exchange was tested using the $OVA_{323\text{-}339}$ peptide from ovalbumin. The cleaved mCLIP-$I\text{-}A^b$ complex was incubated at pH 5 with a 25-fold molar excess of the OVA peptide overnight and analyzed by 2D-LCMS. Under these conditions, the efficiency of this exchange was quite low

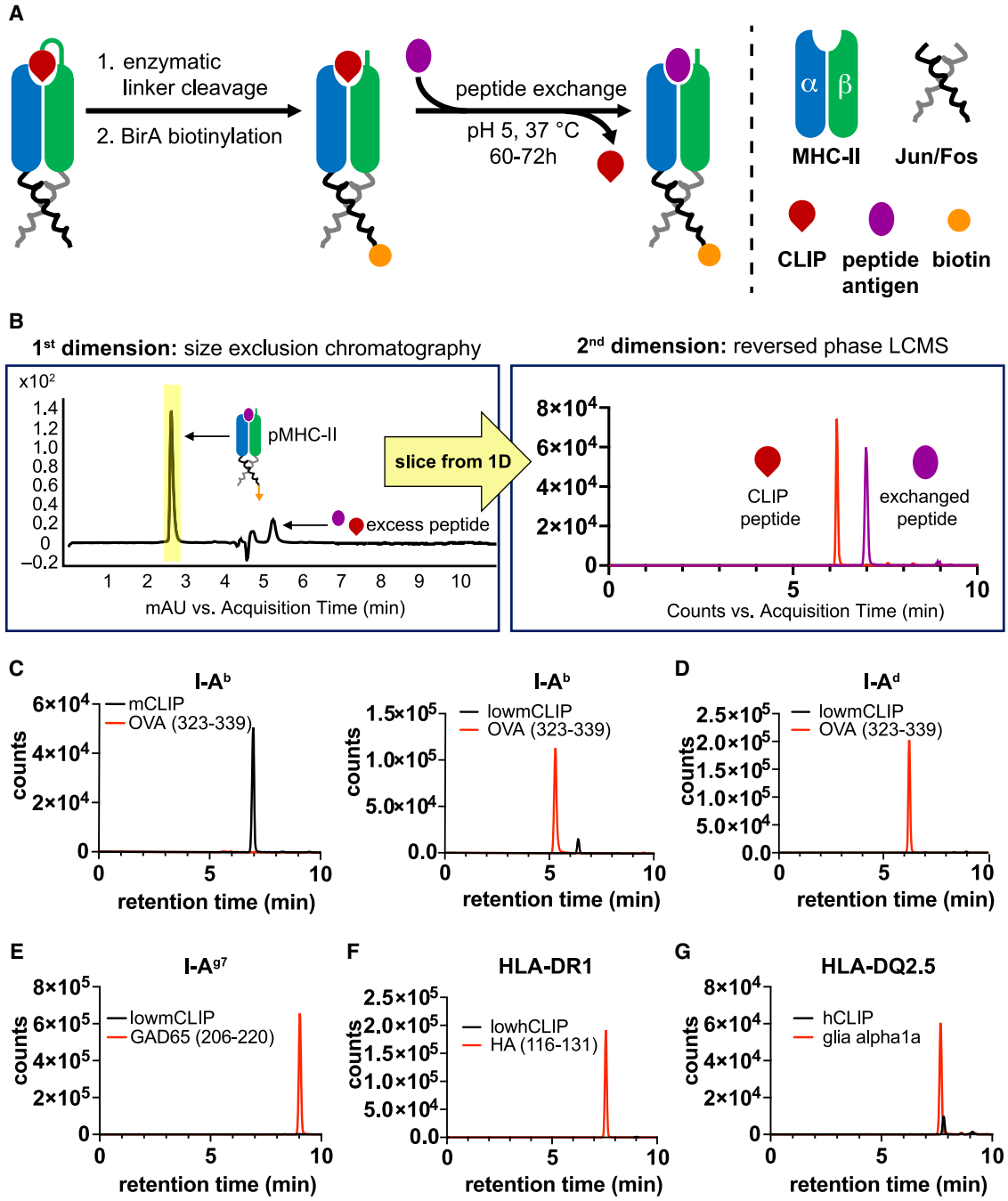

Figure 1. Expression constructs for MHC class II monomers and 2D-LCMS analysis of peptide exchange reactions

(A) MHC-II protein constructs used in these studies (murine and human). pMHC-II with the CLIP peptide (red) undergoes enzymatic linker cleavage using either TEV or thrombin proteases (depending on the linker sequence) to allow peptide exchange with a higher affinity peptide (purple). Biotinylation (depicted as an orange arrow) of pMHC-II allows for subsequent tetramer formation.

(B) Representation of the 2D-LCMS assay: first-dimension with the size exclusion chromatography (SEC) peak isolation and second-dimension with reversed phase LCMS analysis of pMHC-II complexes.

(C) High-affinity mCLIP peptide in the I-A^b allele undergoes very poor peptide exchange with $OVA_{323-339}$ peptide (left panel). A low-affinity mutant mCLIP (lowmCLIP) peptide undergoes efficient peptide exchange with $OVA_{323-339}$ peptide (right panel).

(D) Peptide exchange of the lowmCLIP peptide for the $OVA_{323-339}$ peptide in the I-A^d allele.

(E) Representative peptide exchange of the lowmCLIP peptide for $GAD65_{206-220}$ peptide in the I-A^{g7} allele.

(F) Representative peptide exchange of the lowhCLIP (PVSKARMATGALAQA) for the $HA_{116-131}$ peptide in the HLA-DR1 (i.e., HLA-DRB1*01:01) allele.

(G) Representative peptide exchange of the hCLIP peptide (PVSKMRMATPLLMQA) for the glia alpha1a epitope in the HLA-DQ2.5 allele (i.e., HLA-DQA1*05:01/DQB1*02:01).

A

Peptide Epitope	Sequence	Reported IEDB Affinity (nM)
LCMV NP (201-215)	LGLLYTVKYPNLNDL	1060
LASV RNAP (295-309)	SPILRFLYANVGEEA	503
LCMV RNAP (1840-1854)	YFESFVREFVATART	140
VV HP (23-37)	IVYSLVTTISSLSRI	45
VV VETF (275-289)	DITYKVHLATPINSR	10.2

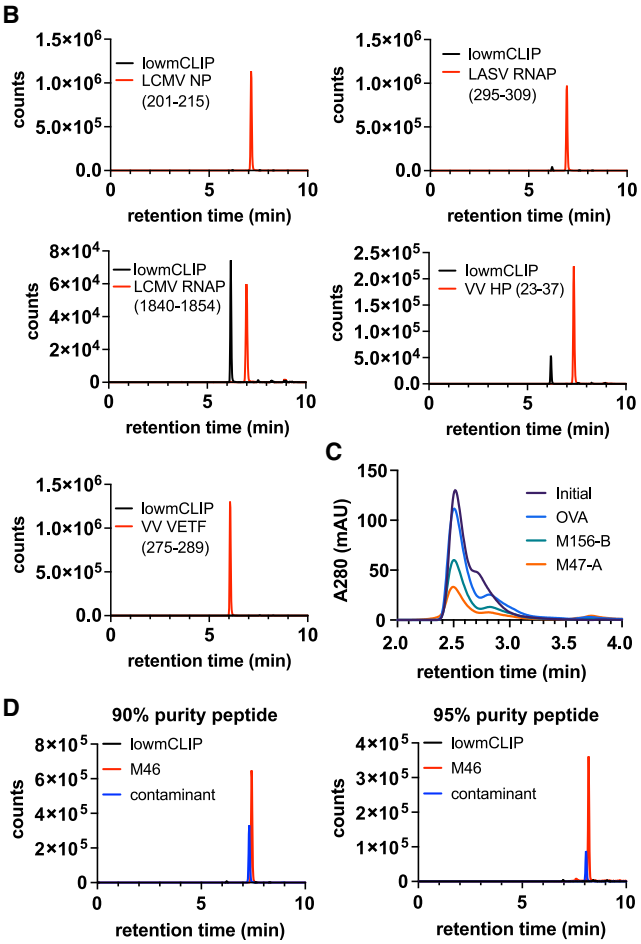

Figure 2. Validation and characterization of the 2D-LCMS method using I-A^b and various peptide epitopes

(A) Table of peptide sequences/epitopes and reported affinities from IEDB.

(B) 2D-LCMS of peptide exchange reactions of the epitopes in (a).

(C) First-dimension SEC analysis of the isolated peak of 4 peptide exchange reactions. An overlay of each reaction is depicted. The initial peak represents data from a sample that was freshly cleaved and diluted to the same concentration as the peptide reaction mixtures. Although OVA peptide led to minimal changes in peak intensity, M156-B and M47-A showed dramatically lower peak areas, suggesting significant precipitation from solution during the exchange reaction.

(D) Peptide exchange of the M46 epitope using either 90% or 95% pure peptide samples. A minor contaminant in this mixture (blue) shows significant peptide exchange.

as demonstrated by the absence of the OVA peptide and a substantial amount of the mCLIP peptide in the intact complexes isolated in the first dimension (Figure 1C, left panel). Despite including longer incubation times, substantial peptide exchange of the mCLIP peptide could not be achieved (not shown). Although we did not evaluate peptide concentrations higher than 400 μM to push the exchange to completion, we reasoned that the high affinity of the mCLIP peptide to I-A^b likely precludes efficient exchange. Inspired by work from the Wucherpfennig lab,[35] we incorporated 4 mutations into the mCLIP peptide (PVSQMRMATPLLMRP) to generate a new low-affinity mCLIP peptide (lowmCLIP, PVSQ**A**RMAT**GA**L**A**RP) that we anticipated would improve the peptide exchange efficiency. This lowmCLIP peptide enabled highly efficient peptide exchange in the presence of OVA$_{323-339}$ peptide without compromising the high expression efficiency of the covalent complex (Figure 1C, right panel). Furthermore, lowmCLIP maintains a high enough affinity to the I-A^b allele to remain intact in the cleaved complex and allow for relative exchange efficiency to be determined by 2D-LCMS. This optimized system allows for direct peptide exchange monitoring in a label-free environment. Importantly, this approach is quite general, and adaptation to other common murine MHC-II alleles (I-A^d, I-A^s, and I-A^{g7}) has also been validated (Figures 1D, 1E, and S2). In addition, this method has been extended to many human alleles (Figures 1F and 1G) by optimizing human CLIP peptide sequences for many common human MHC-II, also called human leukocyte antigens class II (HLA-II) alleles (Table S1). As a final proof of concept, we demonstrated that the peptide exchange and 2D-LCMS analysis are also effective with autoantigens in both human and mouse alleles (Figure S2).

Validation and advantages of 2D-LCMS detection

To further validate the lowmCLIP-I-A^b system, we turned to the IEDB and randomly selected 5 peptides with varying affinities to I-A^b that reportedly ranged from 10 to 1000 nM (Figure 2A). These epitopes were each subjected to peptide exchange for 60 h at pH 5 and analyzed by 2D-LCMS following our standard protocol. All of the peptides demonstrated appreciable levels of exchange; however, the extent of exchange efficiency was not well correlated with the reported peptide affinity (Figure 2B). Although the reason for this discrepancy is not certain, two potential factors could explain these results. First, the reported affinities were determined by indirect detection methods that only account for the displaced peptide in a competition assay and do not confirm formation of a new complex. These assays may overpredict binding in situations where excess peptide may lead to complex destabilization or precipitation without any concomitant peptide exchange. Indeed, our experience with peptide exchange and 2D-LCMS thus far has indicated that many peptides can lead to precipitation of the complex, as indicated by the significantly reduced peak area in the first dimension during the course of a peptide exchange reaction without significant peptide exchange observed (Figure 2C), although it is also possible that the higher concentration used in the 2D-LCMS assay in comparison to other methods increases the propensity for precipitation of poorly soluble peptides. A second possibility concerns the purity of the peptides used for the affinity determinations. In our experiments, we have noted the importance of using peptides of very high purity (95% or greater). We found that in some instances, lower purity peptides

containing minor contaminants from amino acid deletions during synthesis were able to significantly outcompete the desired peptide (Figures 2D and S3A). Because of the ability to definitively identify the peptides by MS, we were able to discriminate between desired and undesired peptides that would be nearly impossible to discern with an indirect detection method. Taken together, these results suggest that this analysis method is superior to conventional competition assays that have been used to characterize peptide binding to MHC-II proteins. Building on this experiment, we have also demonstrated that pooled peptide exchange experiments are possible and provide additional information about peptide binding. When performing peptide exchange with individual peptides derived from the M46 neoantigen, we found that M46-A and M46-B both underwent complete peptide exchange; however, when a pooled analysis of the 4 M46 peptides was performed, M46-A outcompetes M46-B indicating that M46-A has higher affinity than M46-B (Figure S3B). Other variations on pooled peptide analyses are also possible with this method, for example using MHC-II in excess of the competing peptides to determine which peptides are capable of binding from a larger mixture of peptides.

An additional advantage of 2D-LCMS analysis was realized when performing peptide exchange with cysteine-containing peptides dissolved in dimethyl sulfoxide (DMSO). Here, we observed that a fraction of the MHC-II was bound to the corresponding intermolecular or intramolecular disulfide. DMSO is a very commonly used solvent for solubilizing peptides; however, dissolving cysteine-containing peptides in DMSO can lead to rapid disulfide formation (intermolecular for peptides with a single cysteine but also potentially intramolecular for peptides containing multiple cysteines). To overcome this limitation, we instead prepared peptide stock solutions in ethylene glycol, which significantly limits the undesired formation of disulfides. We have found that ethylene glycol has a high dissolving power and is a suitable solvent for dissolving most polar and nonpolar peptides. Additionally, the inclusion of 0.5 mM tris(2-carboxyethyl)phosphine (TCEP) in the reaction mixture keeps cysteine-containing peptides reduced during the peptide exchange reaction, allowing accurate assessment of the linear peptide binding epitope and as well as ensuring the generation of homogeneous pMHC-II for downstream applications. This observation likely would have gone unnoticed if analysis methods relying on indirect detection methods were used.

Purification-free assembly of peptide-exchanged MHC-II multimers

In order to be broadly applicable to immune monitoring, streamlined generation of pMHC-II monomers for assembly into fluorescent-labeled multimers is required. Having established a reliable peptide exchange protocol and 2D-LCMS assay, we next sought to simplify the MHC-II multimerization protocol by removing the monomer purification step. This 1-step protocol combines fluorescent-coupled streptavidin reagent to pMHC monomers for a soluble reagent ready to use after 20 min incubation on ice in the dark for T cell staining.

To further validate this simple protocol with specific T cell staining, we used the M112 mutation that we previously identified in the MC38 murine model,[36,37] and for which we detected

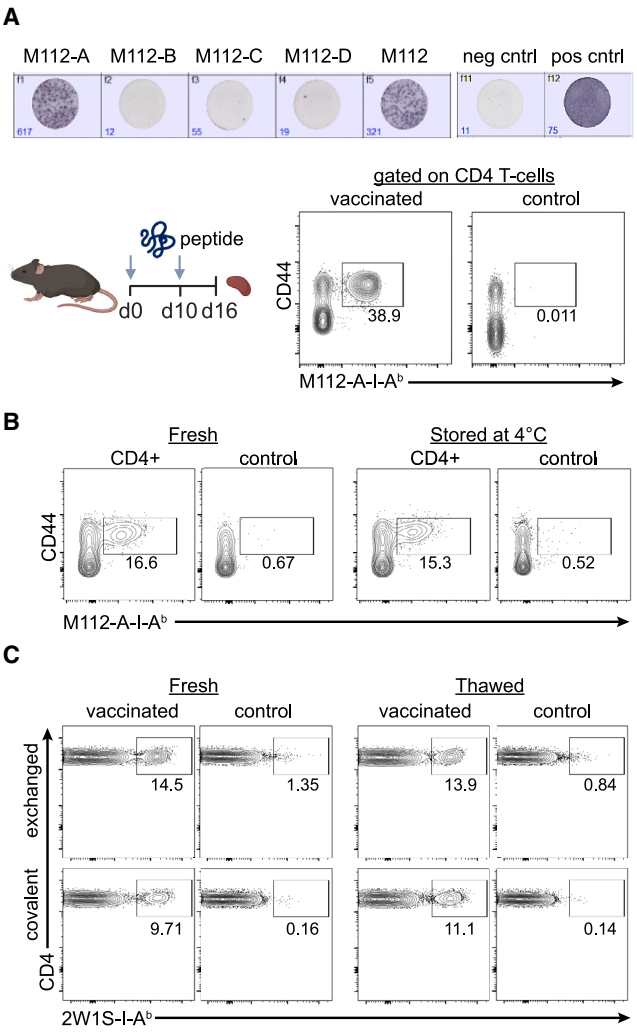

Figure 3. Identifying I-Ab binding neoepitopes to monitor antigen-specific CD4$^+$ T cells

(A) M112 mutation-specific CD4$^+$ T cell response assessed either by IFN-gamma ELISpot assay (post CD8 depletion) or pI-A^b tetramer staining. Splenocytes from mice vaccinated with M112 peptide were restimulated *in vitro* either with mutated 24-aa or 15-aa peptides and assessed for IFN-gamma release. Additionally, splenocytes were enriched for M112-specific CD4$^+$ T cells and analyzed by flow cytometry. Representative ELISpot images and FACS plots are shown.

(B) Representative FACS plot of tetramer staining (M112:I-A^b) from fresh or 1-week-old (stored at 4°C) material of splenocytes from vaccinated animals. CD8$^+$ T cells were used as negative control.

(C) Representative FACS plot of tetramer staining (2W1S:I-A^b) from fresh or frozen material of splenocytes from vaccinated animals with the 2W1S peptide. Covalent tetramers were used as a comparison. Vehicle vaccines were used as control. *In vivo* studies were conducted with $n = 3$ mice per group for all panels in this figure.

a CD4$^+$ T cell response after peptide vaccination in naive mice (Figure 3A, top panel). As the peptide vaccine encoded a 24 aa sequence, we generated overlapping 15 aa peptides shifted by 3 residues between consecutive peptides containing the M112 mutation from the 24-aa sequence (M112-A to D) to be screened for MHC-II binding. Using our strategy described above, only

one epitope (M112-A) out of the 4 tested bound to I-A^b. We confirmed the M112-A specific $CD4^+$ T cell response after re-stimulation of $CD8^+$ T cell-depleted splenocytes from M112 vaccinated mice with each of the 4 epitopes (M112-A-D) by IFN-γ ELISpot assay (Figure 3A, bottom panel; Table S2). Following the standard peptide exchange conditions identified above, the biotinylated monomers containing predominantly M112-A peptide were then added in a 2:1 M excess with respect to streptavidin monomer to fluorescently labeled streptavidin. The assembled PE-labeled M112-A:I-A^b tetramer was then used to stain splenocytes from M112-vaccinated animals, and enrichment of the tetramer-positive population allowed us to clearly identify the M112-A-specific $CD4^+$ T cell population (Figure 3A, bottom panel). Importantly, this protocol for monomer generation can be used with both dextramers and affinity-matured MHC-II reagents that have been engineered to bind the CD4 co-receptor with higher affinity (Figure S1).[38,39]

We further assessed reagent stability using larger batches of purified, biotinylated, and cleaved lowmCLIP-I-A^b monomers after storage for a week (Figure 3B) or a month (not shown) at 4°C, which allows for the preparation of a large stock of monomer for exchange/multimer assembly processes. As covalently-linked peptide fused to the MHC-II beta chain N-terminus is one of the standard methods for generating larger batches of monomers, we next compared cell staining by multimers generated from either peptide-exchanged or covalently-linked monomers. Here, we used the well-characterized 2W1S I-A^b epitope that has been shown to generate a robust immune $CD4^+$ T cell response after immunization.[31,40,41] Simultaneously, we tested the stability of these monomers to freeze-thaw cycles, which would greatly facilitate larger scale multimer production. Similar frequencies of 2W1S-specific $CD4^+$ T cells were detected in spleens of vaccinated mice in all conditions (Figure 3C). As concern over the stability of these non-covalent, exchanged complexes was a key driver in these storage experiments, the fact that they have proven stable and that QC can be performed easily using the 2D-LCMS makes this approach appealing even for pMHC-II complexes that can be prepared from recombinant expression of the covalently fused peptide complex. This result demonstrates the advantage of our strategy (MHC2-SCALE) combining 3 protocols into one simple workflow for generating peptide-specific MHC-II multimers that can be used for immune monitoring, and further characterization of (*neo*) antigen-specific $CD4^+$ T cells.

Peptide exchange enables accurate mapping of T cell epitopes

To further assess the utility of MHC2-SCALE, we evaluated the ability of this assay to map core peptide binding domains derived from tumor mutations previously identified in the MC38 murine model,[36,37] and we determined $CD4^+$ T cell responses *ex vivo* by IFN-γ ELISpot as described previously for the M112 mutation. Most of the 222 mutations identified in Yadav, Nature 2014 showed an absence of MHC-II immunogenicity following restimulation of the cells with the 24 aa long mutated sequences. In order to narrow down the number of epitopes to screen with MHC2-SCALE, we randomly selected 33 mutations that either induced a $CD4^+$ T cell response (13/33) or showed no response (20/33). As previously described for the M112 mutation, we defined four 15 aa epitopes for each of the 33 mutations to be exchanged with lowmCLIP peptide, for a total of 132 peptides of 15 aa length. As one peptide synthesis failed, only 131 out of the 132 peptides were tested for binding using MHC2-SCALE. We found 86 binders, 44 non-binders, and 2 inconclusive results (Table S2). Since IEDB is one of the most common software used to predict binding for MHC molecules, we decided to compare the 2D-LCMS binding data to the predicted binders identified with the publicly available MHC-II IEDB prediction algorithm (recommended version 2.22). The predicted binding score for each of the 132 mutated peptides based on the percentile rank of the 15 aa sequence is reported in Table S2. To define binders and non-binders, we used the current IEDB recommendation based on a consensus percentile rank of the top 20%.[42] Based on this cutoff, we found that 86% (38/44) of the 15 aa peptides in our dataset that were predicted to bind I-A^b (IEDB score $\leq$20) were also binders with MHC2-SCALE (Figure 4A). As a representative example, the only 2 peptides of the M57 mutation that were predicted to bind I-A^b (M57-A and M57-B) were also the only ones detected as binders with MHC2-SCALE (Figure 4C). However, within the predicted non-binding peptide set (IEDB score >20), 56% (49/88) of the peptides were real binders as assessed by MHC2-SCALE (Figure 4B). The case of M112 illustrates this situation well with none of the 4 peptides predicted to bind, while M112-A was identified as a strong binder with MHC2-SCALE (Figure 4D). Since IEDB NetMHCIIpan EL or BA are also common versions used for predicting MHCII epitopes, we also analyzed our dataset using percentile ranks from the recommended NetMHCIIpan EL 4.1 and BA 4.1 versions, and found very similar results (Table S2; Figure S4). This result suggests that MHC2-SCALE is more sensitive than the IEDB tools at identifying binding epitopes.

In order to validate the MHC-II epitopes identified as binders with MHC2-SCALE, we further individually assessed the immunogenicity of 131/132 short 15 aa overlapping peptides of the 33 mutations *ex vivo*. We immunized naive mice with vaccines encoding the 24 aa mutated sequence (peptide or RNA vaccine) and determined the $CD4^+$ T cell response of the four related 15 aa overlapping peptides by restimulating the cells with the 15 aa peptides within the IFN-γ ELISpot assay (Figure 5A). We found that 31/131 mutated peptides were recognized by $CD4^+$ T cells *in vitro* (Table S2). While some data from MHC2-SCALE correlated well with the MHC-II immunogenicity assessment (Figures 5B and 5C), not all peptides identified as binders with MHC2-SCALE induced a $CD4^+$ T cell response as shown with the M57 mutation, independent of the vaccine platform (Figures 4C and 5D). Although all peptides include a mutation, this result was expected since not all neoantigen peptides presented on MHC molecules are recognized as foreign by T cell receptors.[37,43–45] Furthermore, the sensitivity of the ELISpot assay is limited and may not detect weak T cell responses. To evaluate the accuracy of MHC2-SCALE, we reasoned that the 15 aa long mutated peptides stimulating $CD4^+$ T cells *in vitro* needed to bind I-A^b molecules in order to be presented by APCs to T cells present in the splenocyte population isolated from vaccinated mice. We found that more than

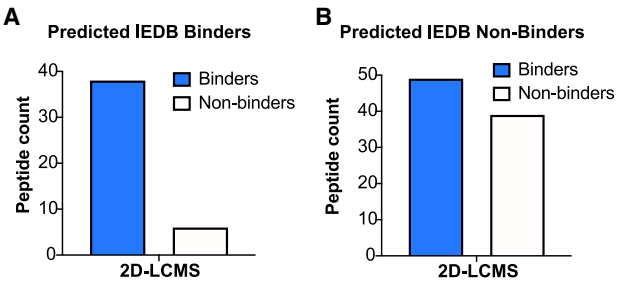

C

Neoantigen	Sequence	IEDB Score
M57	DRGVIMSAHSLT(D/N)SSSDFMEQVST	
M57-A	DRGVIMSAHSLT(D/N)SS	8.75
M57-B	VIMSAHSLT(D/N)SSSDF	14.25
M57-C	SAHSLT(D/N)SSSDFMEQ	37.5
M57-D	SLT(D/N)SSSDFMEQVST	79

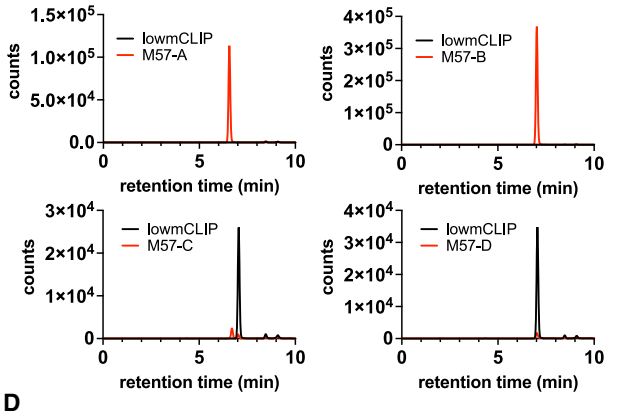

D

Neoantigen	Sequence	IEDB Score
M112	HYKYMCNSSCMG(G/V)MNRRPILTIIT	
M112-A	HYKYMCNSSCMG(G/V)MN	39.5
M112-B	YMCNSSCMG(G/V)MNRRP	66.5
M112-C	NSSCMG(G/V)MNRRPILT	46
M112-D	CMG(G/V)MNRRPILTIIT	27.5

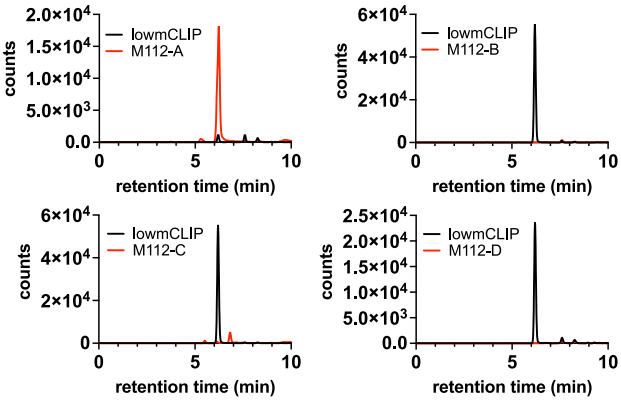

Figure 4. Binding prediction and 2D-LCMS binding assay of mutated peptides derived from the MC38 tumor cell line

(A) Bar graph representing the count of mutated peptides out of the 131 tested peptides that were predicted as binders with IEDB (percentile rank ≤20) and detected as binders or non-binders with the 2D-LCMS assay.

(B) Bar graph representing the count of mutated peptides out of the 131 tested peptides that were predicted as non-binders with IEDB (percentile rank >20) and detected as binders or non-binders with the 2D-LCMS assay.

(C and D) Tables depicting sequences from overlapping 15-aa peptide libraries for the M57 (C) and M112 (D) mutations. aa change is shown in parentheses (WT/MUT). 2D-LCMS graphs for each epitope sequence are shown. Peptides of interest are shown in red, lowmCLIP peptide is shown in black.

77% (24/31) of the MHC-II immunogenic 15 aa mutated peptides were I-A^b binders by MHC2-SCALE (Table S2; Figure 5E). To note, the assessment of binding was inconclusive for 2 peptides, and only 5 cases showed discrepancies between MHC2-SCALE and ELISpot assays (Table S2). One explanation could be due to low peptide purity given that peptides with >70% purity were used to assess immunogenic responses in the ELISpot assay. Peptide contaminants may be responsible for the CD4$^+$ T cell responses, especially since weak responses were observed for most of these peptides. In addition, the high hydrophobicity and low solubility of some of these peptides may have contributed to the lack of binding in the peptide exchange reaction. Importantly, only 52% (16/31) of these neoepitopes inducing a CD4$^+$ T cell response were predicted to bind with the IEDB tool (cons 2.22; Table S2; Figure 5E). We also found similar results with the recommended NetMHCIIpan EL and BA 4.1 (Table S2; Figure S4). This result demonstrates the high sensitivity of the MHC2-SCALE approach to assess MHC-II binding, thus highlighting the utility of the method in providing high-quality datasets that can be used to improve binding prediction algorithms.

DISCUSSION

In this study, we developed a new workflow called MHC2-SCALE to reliably identify both mouse and human MHC-II binding peptides and seamlessly generate fluorescently-labeled multimers for tracking peptide-specific CD4$^+$ T cells by flow cytometry. MHC2-SCALE presents multiple advantages over the current conventional methods.

MHC2-SCALE combines 3 protocols, each optimized, into a simple workflow that can easily be performed in 96-well plate format over the course of 3–4 days with the majority of the time being hands-off and readily amenable to automation with liquid handling instrumentation. In addition, the purification-free multimerization enables generation of multiple milligrams of single tetramer reagents, and with optimal experiment planning, peptide exchange can be started on a Friday morning, and tetramer reagents can be completed by the following Monday afternoon. MHC2-SCALE allows for large scale screening of MHC-II epitope candidates using readily-produced reagents without the need of additional co-factors or purification steps, overcoming some of the most common limitations of other methods used for generating pMHCII molecules, such as recombinant peptide fusion or other peptide exchange protocols. Convenient storage of monomer reagents at 4°C or −80°C

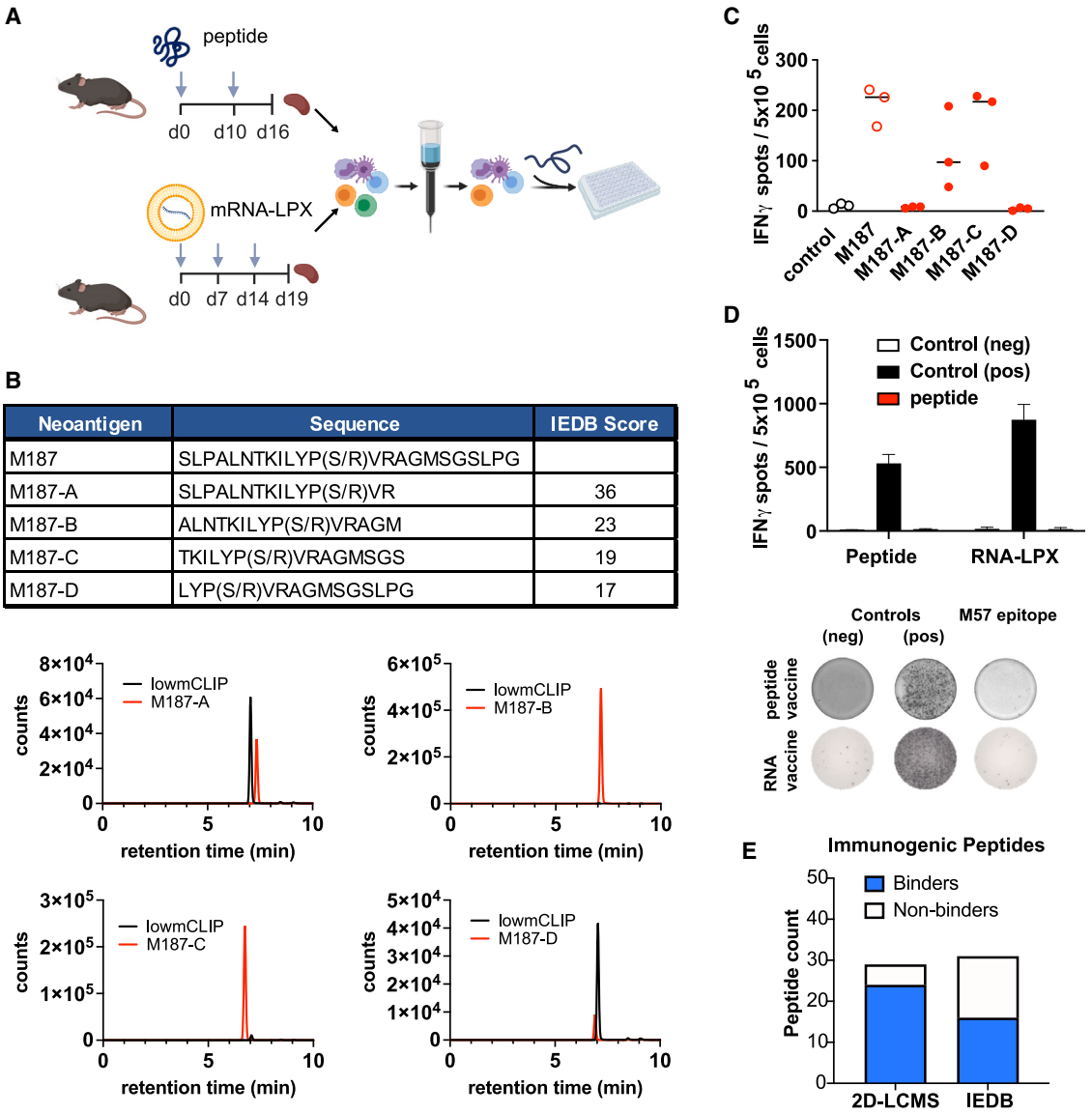

Neoantigen	Sequence	IEDB Score
M187	SLPALNTKILYP(S/R)VRAGMSGSLPG	
M187-A	SLPALNTKILYP(S/R)VR	36
M187-B	ALNTKILYP(S/R)VRAGM	23
M187-C	TKILYP(S/R)VRAGMSGS	19
M187-D	LYP(S/R)VRAGMSGSLPG	17

Figure 5. Immunogenicity of mutated peptides derived from the MC38 tumor cell line

(A) Schema depicting the study design for (c and d). Naive mice were immunized with mutant peptide on days 0 and 10, or mRNA-LPX vaccine on days 0, 7, and 14. $CD4^+$ T cell responses were assessed in the spleen 5 or 6 days following the last immunization by IFN-gamma ELISpot (after $CD8^+$ T cell depletion). $n = 3$ mice were used for each group.

(B) Table depicting sequences from overlapping 15-aa peptide libraries for the M187 mutation. aa change is shown in parentheses (WT/MUT). 2D-LCMS graphs for each epitope sequence are shown. Peptides of interest are shown in red and lowmCLIP peptide is shown in black.

(C and D) Splenocytes from vaccinated mice ($n = 3$) were depleted of $CD8^+$ T cells and incubated overnight with peptides for assessing T cell stimulation with IFN-gamma ELISpot assay. Absence of peptide was used as a negative control and CD3/CD28 Dynabeads (Gibco) as a positive control for T cell stimulation. In (C), peptide-vaccinated splenocytes were incubated either with 24-aa (M187) or overlapping 15-aa peptides (M187-A to D). Data are plotted as the mean with individual replicates displayed as circles. In (D), splenocytes from mice ($n = 3$) vaccinated with the 24-aa peptide or with RNA-LPX encoding the 24-aa peptide were restimulated with the 24-aa peptide within the ELISpot assay. No specific $CD4^+$ T cell response was observed for either vaccine platform. Data are presented as mean ± SD.

(E) Bar graph representing the count of immunogenic mutated peptides out of the 131 tested peptides that were detected as binder/non-binder with the 2D-LCMS assay, or predicted as binder/non-binder with IEDB (percentile rank; cutoff 20). A total of 31 mutated peptides were determined as MHC-II immunogenic and predicted to bind to $I\text{-}A^b$ by the IEDB. Only 29 mutated peptides were assessed for $I\text{-}A^b$ binding using the 2D-LCMS method due to failure of peptide synthesis.

and a simple fluorescently-labeled multimerization step enables screening, detection, and deep characterization of antigen-specific $CD4^+$ T cells *ex vivo*.

Furthermore, MHC2-SCALE increases MHC-II binding accuracy and sensitivity. While peptide binding assays are commonly used for epitope screening and can be high-throughput, our

strategy allows identification and exclusion of impurities that can create false positives in conventional binding assays by using an unbiased 2D-LCMS analysis step. On the other hand, peptides with low affinity for MHC-II molecules may not be detected efficiently with some conventional peptide binding assays, leading to false negatives. In comparison to the MHC-II IEDB algorithm, which is mostly based on datasets generated from peptide binding assays,[46] our approach shows a 25% increase at detecting real binders within an immunogenic peptide dataset. Indeed, it is widely recognized that MHC-II binding prediction algorithms suffer from much lower accuracy than their MHC-I counterparts. We have demonstrated that MHC2-SCALE, when paired with immunogenicity screening assays, discriminates between MHC-II immunogenic and non-immunogenic mutated peptides that bind to I-A^b, while immunogenic epitopes were often not predicted to bind by IEDB scoring. Thus, we believe that MHC2-SCALE provides a blueprint for improving dataset quality for immunogenicity prediction of MHC-II epitopes, and selection of tumor-specific antigens for targeted therapy.

MHC2-SCALE can also be used for broader peptide sequences and many different murine and human alleles. Our strategy has been optimized for the use of cysteine-containing peptides that are challenging to produce by conventional direct fusion methods. Indeed, poorly expressing or lower-affinity peptides require cysteine trapping technologies to increase expression yields, which is unsuitable for peptides naturally containing cysteines. By optimizing the peptide dissolution solvent, including TCEP during the peptide exchange reaction, and using 2D-LCMS for analysis, identification of discrete peptide binding motifs of cysteine-containing peptides has been enabled. To date, we have extended this protocol across multiple murine alleles as well as human HLA-DR, DQ, and DP alleles with great success, highlighting the generality of the overall workflow. Beyond its generality, this approach also provides significantly cheaper custom-made tetramers compared to most methods, especially compared to commercially available product kits. Thus, the MHC2-SCALE approach is expected to become increasingly attractive to academic labs with LCMS instrumentation becoming ever more available and powerful.

In conclusion, MHC2-SCALE is a universal workflow that accommodates most peptide sequences and is more reliable, more reproducible, less time-consuming, and more economical than common methods, thus demonstrating the utility and advantage of MHC2-SCALE over standard methods for generating peptide-specific MHC-II multimers. This strategy also opens new opportunities for characterizing antigen-specific $CD4^+$ T cell responses in a broader context of targeted immunotherapy, including cancer, autoimmunity, and infectious diseases.

Limitations of the study

One limitation of the MHC2-SCALE approach is its reliance on MHC-II binding assessment. Peptides with high hydrophobicity and low solubility may exhibit reduced binding to MHC-II during the peptide exchange reaction due to concomitant precipitation of the MHC complex, potentially leading to an increased rate of false negatives with the MH2-SCALE method. Our protocol has been optimized to include cysteine-containing peptides and enhance the dissolution of hydrophobic peptides. However, further research is needed to identify a universal solvent/buffer system that can effectively accommodate all peptide sequences.

Additionally, we validated our method using a pool of immunogenic peptides identified through ELISpot assay after *in vivo* immunization. Although we demonstrated that these MHC-II epitopes are naturally processed by APCs, presented to CD4 T cells, and capable of inducing activation and expansion of CD4 T cells in mice (via immunization with long peptide), we did not investigate whether these epitopes are also presented on MHC-II molecules on the surface of MC38 tumor cells. This information as well as future work studying the specific CD4 T cell responses in tumor-bearing animals would be required for fully establishing the relevance of these neoantigen candidates for targeted-immunotherapy.

RESOURCE AVAILABILITY

Lead contact

Further information and requests for resources and reagents should be directed to the lead contact Adel M. ElSohly (elsohly.adel@gene.com).

Materials availability

Reasonable requests for MHCII reagents can be made available upon request to the lead contact under a material transfer agreement with Genentech, Inc.

Data and code availability

- No original code was developed for this study.
- All data reported in this manuscript will be shared by the lead contact upon request.
- Any additional information necessary to reanalyze the data presented in this manuscript will be made available upon request to the lead contact.

ACKNOWLEDGMENTS

We thank Jieming Chen for his review of the manuscript and helpful comments. We acknowledge technical support from BioRender with the graphical abstract and manuscript Figures 3 and 5. All funding was provided by Genentech, Inc.

AUTHOR CONTRIBUTIONS

J.G.G., A.-H.C., and A.M.E. designed research; J.G.G., A-H.C., R.H., R.V., M.D., and J.L.L. performed research; J.G.G. and A.-H.C. analyzed data; A.M.E., A.-H.C., and J.G.G. wrote the manuscript; L.D. and J.L.L. reviewed the manuscript; A.-H.C. and A.M.E. led the project.

DECLARATION OF INTERESTS

All authors are employees of Genentech. A.M.E. and J.G.G. are inventors on a patent filing related to assays and reagents for MHC-II peptide binding.

STAR★METHODS

Detailed methods are provided in the online version of this paper and include the following:

- KEY RESOURCES TABLE
- EXPERIMENTAL MODEL AND STUDY PARTICIPANT DETAILS
  - Mice
  - *In vivo* immunization
- METHOD DETAILS
  - Construct design
  - Protein expression and purification
  - Peptides for 2D-LCMS screening and tetramer generation
  - Buffer exchange

SUPPLEMENTAL INFORMATION

Supplemental information can be found online at https://doi.org/10.1016/j.isci.2025.112212.

Received: September 25, 2024
Revised: December 13, 2024
Accepted: March 10, 2025
Published: March 13, 2025

REFERENCES

1. DuPage, M., and Bluestone, J.A. (2016). Harnessing the plasticity of CD4+ T cells to treat immune-mediated disease. Nat. Rev. Immunol. *16*, 149–163. https://doi.org/10.1038/nri.2015.18.
2. Zhang, L., Conejo-Garcia, J.R., Katsaros, D., Gimotty, P.A., Massobrio, M., Regnani, G., Makrigiannakis, A., Gray, H., Schlienger, K., Liebman, M.N., et al. (2003). Intratumoral T Cells, Recurrence, and Survival in Epithelial Ovarian Cancer. N. Engl. J. Med. *348*, 203–213. https://doi.org/10.1056/NEJMoa020177.
3. Galon, J., Costes, A., Sanchez-Cabo, F., Kirilovsky, A., Mlecnik, B., Lagorce-Pagès, C., Tosolini, M., Camus, M., Berger, A., Wind, P., et al. (2006). Type, Density, and Location of Immune Cells Within Human Colorectal Tumors Predict Clinical Outcome. Science *313*, 1960–1964. https://doi.org/10.1126/science.1129139.
4. Jordanova, E.S., Gorter, A., Ayachi, O., Prins, F., Durrant, L.G., Kenter, G.G., van der Burg, S.H., and Fleuren, G.J. (2008). Human Leukocyte Antigen Class I, MHC Class I Chain-Related Molecule A, and CD8+/Regulatory T-Cell Ratio: Which Variable Determines Survival of Cervical Cancer Patients? Clin. Cancer Res. *14*, 2028–2035. https://doi.org/10.1158/1078-0432.CCR-07-4554.
5. Au, K.K., Le Page, C., Ren, R., Meunier, L., Clément, I., Tyrishkin, K., Peterson, N., Kendall-Dupont, J., Childs, T., Francis, J.-A., et al. (2016). STAT1-associated intratumoural TH1 immunity predicts chemotherapy resistance in high-grade serous ovarian cancer. J. Pathol. Clin. Res. *2*, 259–270. https://doi.org/10.1002/cjp2.55.
6. Laheurte, C., Dosset, M., Vernerey, D., Boullerot, L., Gaugler, B., Gravelin, E., Kaulek, V., Jacquin, M., Cuche, L., Eberst, G., et al. (2019). Distinct prognostic value of circulating anti-telomerase CD4+ Th1 immunity and exhausted PD-1+/TIM-3+ T cells in lung cancer. Br. J. Cancer *121*, 405–416. https://doi.org/10.1038/s41416-019-0531-5.
7. Bruni, D., Angell, H.K., and Galon, J. (2020). The immune contexture and Immunoscore in cancer prognosis and therapeutic efficacy. Nat. Rev. Cancer *20*, 662–680. https://doi.org/10.1038/s41568-020-0285-7.
8. Richardson, J.R., Schöllhorn, A., Gouttefangeas, C., and Schuhmacher, J. (2021). CD4+ T Cells: Multitasking Cells in the Duty of Cancer Immunotherapy. Cancers *13*, 596. https://doi.org/10.3390/cancers13040596.
9. Han, S., Toker, A., Liu, Z.Q., and Ohashi, P.S. (2019). Turning the Tide Against Regulatory T Cells. Front. Oncol. *9*, 279.
10. Tay, R.E., Richardson, E.K., and Toh, H.C. (2021). Revisiting the role of CD4+ T cells in cancer immunotherapy—new insights into old paradigms. Cancer Gene Ther. *28*, 5–17. https://doi.org/10.1038/s41417-020-0183-x.
11. Tran, E., Turcotte, S., Gros, A., Robbins, P.F., Lu, Y.-C., Dudley, M.E., Wunderlich, J.R., Somerville, R.P., Hogan, K., Hinrichs, C.S., et al. (2014). Cancer immunotherapy based on mutation-specific CD4+ T cells in a patient with epithelial cancer. Science *344*, 641–645. https://doi.org/10.1126/science.1251102.
12. Ott, P.A., Hu, Z., Keskin, D.B., Shukla, S.A., Sun, J., Bozym, D.J., Zhang, W., Luoma, A., Giobbie-Hurder, A., Peter, L., et al. (2017). An immunogenic personal neoantigen vaccine for patients with melanoma. Nature *547*, 217–221. https://doi.org/10.1038/nature22991.
13. Sahin, U., Derhovanessian, E., Miller, M., Kloke, B.-P., Simon, P., Löwer, M., Bukur, V., Tadmor, A.D., Luxemburger, U., Schrörs, B., et al. (2017). Personalized RNA mutanome vaccines mobilize poly-specific therapeutic immunity against cancer. Nature *547*, 222–226. https://doi.org/10.1038/nature23003.
14. Lu, Y.-C., Parker, L.L., Lu, T., Zheng, Z., Toomey, M.A., White, D.E., Yao, X., Li, Y.F., Robbins, P.F., Feldman, S.A., et al. (2017). Treatment of Patients With Metastatic Cancer Using a Major Histocompatibility Complex Class II-Restricted T-Cell Receptor Targeting the Cancer Germline Antigen MAGE-A3. J. Clin. Oncol. *35*, 3322–3329. https://doi.org/10.1200/JCO.2017.74.5463.
15. Veatch, J.R., Singhi, N., Srivastava, S., Szeto, J.L., Jesernig, B., Stull, S.M., Fitzgibbon, M., Sarvothama, M., Yechan-Gunja, S., James, S.E., and Riddell, S.R. (2021). A therapeutic cancer vaccine delivers antigens and adjuvants to lymphoid tissues using genetically modified T cells. J. Clin. Investig. *131*, e144195. https://doi.org/10.1172/JCI144195.
16. Crawford, F., Kozono, H., White, J., Marrack, P., and Kappler, J. (1998). Detection of antigen-specific T cells with multivalent soluble class II MHC covalent peptide complexes. Immunity *8*, 675–682. https://doi.org/10.1016/s1074-7613(00)80572-5.
17. Kozono, H., White, J., Clements, J., Marrack, P., and Kappler, J. (1994). Production of soluble MHC class II proteins with covalently bound single peptides. Nature *369*, 151–154. https://doi.org/10.1038/369151a0.
18. Day, C.L., Seth, N.P., Lucas, M., Appel, H., Gauthier, L., Lauer, G.M., Robbins, G.K., Szczepiorkowski, Z.M., Casson, D.R., Chung, R.T., et al. (2003). Ex vivo analysis of human memory CD4 T cells specific for hepatitis C virus using MHC class II tetramers. J. Clin. Investig. *112*, 831–842. https://doi.org/10.1172/JCI18509.
19. Jang, M.-H., Seth, N.P., and Wucherpfennig, K.W. (2003). Ex Vivo Analysis of Thymic CD4 T Cells in Nonobese Diabetic Mice with Tetramers Generated from I-Ag7/Class II-Associated Invariant Chain Peptide Precursors 1. J. Immunol. *171*, 4175–4186. https://doi.org/10.4049/jimmunol.171.8.4175.
20. Stadinski, B.D., Zhang, L., Crawford, F., Marrack, P., Eisenbarth, G.S., and Kappler, J.W. (2010). Diabetogenic T cells recognize insulin bound to IAg7 in an unexpected, weakly binding register. Proc. Natl. Acad. Sci. USA *107*, 10978–10983. https://doi.org/10.1073/pnas.1006545107.
21. Vyasamneni, R., Kohler, V., Karki, B., Mahimkar, G., Esaulova, E., McGee, J., Kallin, D., Sheen, J.H., Harjanto, D., Kirsch, M., et al. (2023). A universal MHCII technology platform to characterize antigen-specific CD4+ T cells. Cell Rep. Methods *3*, 100388. https://doi.org/10.1016/j.crmeth.2022.100388.
22. Willis, R.A., Ramachandiran, V., Shires, J.C., Bai, G., Jeter, K., Bell, D.L., Han, L., Kazarian, T., Ugwu, K.C., Laur, O., et al. (2021). Production of Class II MHC Proteins in Lentiviral Vector-Transduced HEK-293T Cells for Tetramer Staining Reagents. Curr. Protoc. *1*, e36. https://doi.org/10.1002/cpz1.36.
23. Denzin, L.K., and Cresswell, P. (1995). HLA-DM induces CLIP dissociation from MHC class II alpha beta dimers and facilitates peptide loading. Cell *82*, 155–165. https://doi.org/10.1016/0092-8674(95)90061-6.
24. Sloan, V.S., Cameron, P., Porter, G., Gammon, M., Amaya, M., Mellins, E., and Zaller, D.M. (1995). Mediation by HLA-DM of dissociation of peptides from HLA-DR. Nature *375*, 802–806. https://doi.org/10.1038/375802a0.

25. Sherman, M.A., Weber, D.A., and Jensen, P.E. (1995). DM enhances peptide binding to class II MHC by release of invariant chain-derived peptide. Immunity *3*, 197–205. https://doi.org/10.1016/1074-7613(95)90089-6.

26. Nanaware, P.P., Jurewicz, M.M., Leszyk, J.D., Shaffer, S.A., and Stern, L.J. (2019). HLA-DO Modulates the Diversity of the MHC-II Self-peptidome. Mol. Cell. Proteomics *18*, 490–503. https://doi.org/10.1074/mcp.RA118.000956.

27. Stern, L.J., and Wiley, D.C. (1992). The human class II MHC protein HLA-DR1 assembles as empty alpha beta heterodimers in the absence of antigenic peptide. Cell *68*, 465–477. https://doi.org/10.1016/0092-8674(92)90184-e.

28. Scott, C.A., Garcia, K.C., Carbone, F.R., Wilson, I.A., and Teyton, L. (1996). Role of chain pairing for the production of functional soluble IA major histocompatibility complex class II molecules. J. Exp. Med. *183*, 2087–2095. https://doi.org/10.1084/jem.183.5.2087.

29. Scott, C.A., Garcia, K.C., Stura, E.A., Peterson, P.A., Wilson, I.A., and Teyton, L. (1998). Engineering protein for X-ray crystallography: the murine Major Histocompatibility Complex class II molecule I-Ad. Protein Sci. *7*, 413–418. https://doi.org/10.1002/pro.5560070222.

30. Henderson, K.N., Reid, H.H., Borg, N.A., Broughton, S.E., Huyton, T., Anderson, R.P., McCluskey, J., and Rossjohn, J. (2007). The production and crystallization of the human leukocyte antigen class II molecules HLA-DQ2 and HLA-DQ8 complexed with deamidated gliadin peptides implicated in coeliac disease. Acta Crystallogr., Sect. F: Struct. Biol. Cryst. Commun. *63*, 1021–1025. https://doi.org/10.1107/S1744309107051408.

31. Moon, J.J., Chu, H.H., Pepper, M., McSorley, S.J., Jameson, S.C., Kedl, R.M., and Jenkins, M.K. (2007). Naive CD4(+) T cell frequency varies for different epitopes and predicts repertoire diversity and response magnitude. Immunity *27*, 203–213. https://doi.org/10.1016/j.immuni.2007.07.007.

32. Darwish, M., Wichner, S., Li, J., Chang, J.C., Tam, C., Franke, Y., Li, H., Chan, P., and Blanchette, C. (2021). High-throughput identification of conditional MHCI ligands and scaled-up production of conditional MHCI complexes. Protein Sci. *30*, 1169–1183. https://doi.org/10.1002/pro.4082.

33. Kong, Y., Rose, C.M., Cass, A.A., Williams, A.G., Darwish, M., Lianoglou, S., Haverty, P.M., Tong, A.-J., Blanchette, C., Albert, M.L., et al. (2019). Transposable element expression in tumors is associated with immune infiltration and increased antigenicity. Nat. Commun. *10*, 5228. https://doi.org/10.1038/s41467-019-13035-2.

34. Schachner, L.F., Phung, W., Han, G., Darwish, M., Bell, A., Mellors, J.S., Srzentic, K., Huguet, R., Blanchette, C., and Sandoval, W. (2022). High-Throughput, Quantitative Analysis of Peptide-Exchanged MHCI Complexes by Native Mass Spectrometry. Anal. Chem. *94*, 14593–14602. https://doi.org/10.1021/acs.analchem.2c02423.

35. Anders, A.-K., Call, M.J., Schulze, M.-S.E.D., Fowler, K.D., Schubert, D.A., Seth, N.P., Sundberg, E.J., and Wucherpfennig, K.W. (2011). HLA-DM captures partially empty HLA-DR molecules for catalyzed removal of peptide. Nat. Immunol. *12*, 54–61. https://doi.org/10.1038/ni.1967.

36. Yadav, M., Jhunjhunwala, S., Phung, Q.T., Lupardus, P., Tanguay, J., Bumbaca, S., Franci, C., Cheung, T.K., Fritsche, J., Weinschenk, T., et al. (2014). Predicting immunogenic tumour mutations by combining mass spectrometry and exome sequencing. Nature *515*, 572–576. https://doi.org/10.1038/nature14001.

37. Capietto, A.-H., Jhunjhunwala, S., Pollock, S.B., Lupardus, P., Wong, J., Hänsch, L., Cevallos, J., Chestnut, Y., Fernandez, A., Lounsbury, N., et al. (2020). Mutation position is an important determinant for predicting cancer neoantigens. J. Exp. Med. *217*, e20190179. https://doi.org/10.1084/jem.20190179.

38. Sugata, K., Matsunaga, Y., Yamashita, Y., Nakatsugawa, M., Guo, T., Halabelian, L., Ohashi, Y., Saso, K., Rahman, M.A., Anczurowski, M., et al. (2021). Affinity-matured HLA class II dimers for robust staining of antigen-specific CD4+ T cells. Nat. Biotechnol. *39*, 958–967. https://doi.org/10.1038/s41587-021-00836-4.

39. Dileepan, T., Malhotra, D., Kotov, D.I., Kolawole, E.M., Krueger, P.D., Evavold, B.D., and Jenkins, M.K. (2021). MHC class II tetramers engineered for enhanced binding to CD4 improve detection of antigen-specific T cells. Nat. Biotechnol. *39*, 943–948. https://doi.org/10.1038/s41587-021-00893-9.

40. Rudensky, A., Preston-Hurlburt, P., Hong, S.-C., Barlow, A., and Janeway, C.A. (1991). Sequence analysis of peptides bound to MHC class II molecules. Nature *353*, 622–627. https://doi.org/10.1038/353622a0.

41. Rees, W., Bender, J., Teague, T.K., Kedl, R.M., Crawford, F., Marrack, P., and Kappler, J. (1999). An inverse relationship between T cell receptor affinity and antigen dose during CD4(+) T cell responses *in vivo* and *in vitro*. Proc. Natl. Acad. Sci. USA *96*, 9781–9786. https://doi.org/10.1073/pnas.96.17.9781.

42. Paul, S., Lindestam Arlehamn, C.S., Scriba, T.J., Dillon, M.B.C., Oseroff, C., Hinz, D., McKinney, D.M., Carrasco Pro, S., Sidney, J., Peters, B., and Sette, A. (2015). Development and validation of a broad scheme for prediction of HLA class II restricted T cell epitopes. J. Immunol. Methods *422*, 28–34. https://doi.org/10.1016/j.jim.2015.03.022.

43. Capietto, A.-H., Jhunjhunwala, S., and Delamarre, L. (2017). Characterizing neoantigens for personalized cancer immunotherapy. Curr. Opin. Immunol. *46*, 58–65. https://doi.org/10.1016/j.coi.2017.04.007.

44. Schumacher, T.N., and Schreiber, R.D. (2015). Neoantigens in cancer immunotherapy. Science *348*, 69–74. https://doi.org/10.1126/science.aaa4971.

45. Iizumi, S., Ohtake, J., Murakami, N., Kouro, T., Kawahara, M., Isoda, F., Hamana, H., Kishi, H., Nakamura, N., and Sasada, T. (2019). Identification of Novel HLA Class II-Restricted Neoantigens Derived from Driver Mutations. Cancers *11*, 266. https://doi.org/10.3390/cancers11020266.

46. Wang, P., Sidney, J., Dow, C., Mothé, B., Sette, A., and Peters, B. (2008). A Systematic Assessment of MHC Class II Peptide Binding Predictions and Evaluation of a Consensus Approach. PLoS Comput. Biol. *4*, e1000048. https://doi.org/10.1371/journal.pcbi.1000048.

47. Kranz, L.M., Diken, M., Haas, H., Kreiter, S., Loquai, C., Reuter, K.C., Meng, M., Fritz, D., Vascotto, F., Hefesha, H., et al. (2016). Systemic RNA delivery to dendritic cells exploits antiviral defence for cancer immunotherapy. Nature *534*, 396–401. https://doi.org/10.1038/nature18300.

48. Kwon, K., and Beckett, D. (2000). Function of a conserved sequence motif in biotin holoenzyme synthetases. Protein Sci. *9*, 1530–1539. https://doi.org/10.1110/ps.9.8.1530.

49. Fairhead, M., and Howarth, M. (2015). Site-Specific Biotinylation of Purified Proteins Using BirA. In Site-Specific Protein Labeling: Methods and Protocols Methods in Molecular Biology, A. Gautier and M.J. Hinner, eds. (Springer), pp. 171–184. https://doi.org/10.1007/978-1-4939-2272-7_12.

50. Kapust, R.B., Tözsér, J., Fox, J.D., Anderson, D.E., Cherry, S., Copeland, T.D., and Waugh, D.S. (2001). Tobacco etch virus protease: mechanism of autolysis and rational design of stable mutants with wild-type catalytic proficiency. Protein Eng. Des. Sel. *14*, 993–1000. https://doi.org/10.1093/protein/14.12.993.

STAR★METHODS

KEY RESOURCES TABLE

REAGENT or RESOURCE	SOURCE	IDENTIFIER
Antibodies		
anti-CD40 Ab	Genentech	FGK45
anti-CD90.2 FITC	BD Biosciences	Cat#553004; RRID: AB_394543
anti-CD4 APC-Cy7	BD Biosciences	Cat#552051; RRID: AB_394331
anti-CD8b PerCP-Cy5.5	BD Biosciences	Cat#567597; RRID: AB_2916660
anti-CD44 AF700	BioLegend	Cat#103026; RRID: AB_493713
anti-I-A/I-E BV421	BioLegend	Cat#107631; RRID: AB_10900075
anti-CD11b BV421	BioLegend	Cat#101235; RRID: AB_10897942
anti-CD11c BV421	BioLegend	Cat#117329; RRID: AB_10897814
anti-F4/80 BV421	BioLegend	Cat#123131; RRID: AB_10901171
anti-TCRgd BV421	BioLegend	Cat#118119; RRID: AB_10896753
Chemicals, peptides, and recombinant proteins		
Custom Peptides	JPT	N/A
Custom Peptides	ElimBiopharma	N/A
Custom Peptides	GenScript	N/A
Custom Peptides	AnaSpec	N/A
Streptavidin-PE	BioLegend	Cat#405203
Streptavidin-APC	BioLegend	Cat#405207
Streptavidin-PE	Agilent	Cat#PJRS25
Streptavidin-APC	Agilent	Cat#PJ25S
penicillin/streptomycin	Gibco	Cat#15140122
HEPES	Gibco	Cat#15630130
GlutaMax	Gibco	Cat#35050061
Sodium Pyruvate	Gibco	Cat#11360070
Hanks' Balanced Salt Solution	Gibco	Cat#14025092
Recombinant TEV	Genentech	N/A
Recombinant BirA	Genentech	N/A
Recombinant pMHC molecules	This work	N/A
Critical commercial assays		
96 well ELISpot plate	R&D Systems	Cat#EL485
Experimental models: Organisms/strains		
Female C57BL/6 mice	The Jackson Laboratory	RRID: IMSR_JAX:000664
Oligonucleotides		
poly(I:C)	InvivoGen	Cat#tlrl-picw
Software and algorithms		
Agilent MassHunter Quantitative Analysis	Agilent	N/A
Prism 10	GraphPad	N/A
IEDB algorithm	IEDB.org	http://tools.iedb.org/mhcii/
FlowJo	FlowJo LLC	flowjo.com
BioRender	Biorender	biorender.com
Other		
HisTrap Excel column	Cytiva	Cat#17371206
10K MWCO Amicon centrifugal filter	Millipore Sigma	Cat#UFC901008
Superdex 200 10/300 GL column	Cytiva	Cat#28990944

(*Continued on next page*)

Continued

REAGENT or RESOURCE	SOURCE	IDENTIFIER
2-mL 7K MWCO Zeba desalting column	Thermo Scientific	Cat#89889
Thrombin agarose	Sigma	Cat# RECOMT-1KT
Analytical size exclusion column	Sepax	Cat#213100-4615
Reverse phase PLRP-S column	Agilent	Cat#PL1912-1802
AdvanceBio Peptide Plus column	Agilent	Cat#695775-949
CD8a Ly2 microbeads	Miltenyi	Cat#130-117-044
LS columns	Miltenyi	Cat#130-042-401
anti-PE microbeads	Miltenyi	Cat#130-048-801
anti-APC microbeads	Miltenyi	Cat#130-090-855
Live/Dead Blue Stain	Invitrogen	Cat#L23105
mRNA-LPX	Genentech	N/A

EXPERIMENTAL MODEL AND STUDY PARTICIPANT DETAILS

Mice

Animals were maintained in accordance with the Guide for the Care and Use of Laboratory Animals (National Research Council 2011). Genentech is an AAALAC-accredited facility and all animal activities in this research study were approved by the Genentech Institutional Animal Care and Use Committee (IACUC; 20–0608).

Mice were housed in individually ventilated cages within animal rooms maintained on a 14:10-hour, light:dark cycle. Animal rooms were temperature and humidity-controlled, between 68 to 79°F (20.0 to 26.1°C) and 30 to 70% respectively, with 10 to 15 room air exchanges per hour. All *in vivo* studies were conducted with n=3 mice per group.

In vivo immunization

In order to identify MHC-II epitopes, age-matched 8-10-week-old female C57BL/6 (The Jackson Laboratory; IMSR_JAX:000664) were immunized with mutation-specific peptides derived from MC38 and previously identified and described in Capietto et al. JEM 2020.[37] Briefly, long synthetic peptides (24 AA, 100 μg), in combination with adjuvant (50 μg anti-CD40 Ab clone FGK45 (Genentech) and 100 μg poly(I:C) (InvivoGen, Cat#tlrl-picw) in PBS, were intraperitoneally injected twice 10 days apart. Splenocytes were isolated 6 days later for *ex vivo* assays. In some cases (see figure legends), mRNA-LPX (50 μg) encoding a single neoantigen was injected 7 days apart for a total of 3 intravenous vaccinations.[47] Spleens were harvested 5 days post last vaccine. In order to compare peptide-exchanged and covalent tetramers, we used the 2W1S variant peptide (EAWGALANWAVDSA)[31,40,41] that binds to the I-A^b allele.

METHOD DETAILS

Construct design

The protein sequences of the murine H2-IA^b (α chain UniProt: P14434, β chain UniProt: P14483), H2-IA^d (α chain UniProt: P04228, β chain Uniprot: P01921), H2-IA^s (α chain UniProt: P14437, β chain UniProt: P06345), and H2-IA^{g7} (α chain UniProt: P04228, β chain NCBI: AAA39547.1) alleles were obtained from the referenced accessions, and the protein sequences of the human DR and DQ2.5 alleles were obtained from hla.alleles.org. For each allele, the genes for the extracellular domains of the MHC-II alpha chain and beta chain were codon optimized and cloned into a mammalian expression vector under the control of a CMV promoter. A P2A self-cleaving peptide sequence was inserted between the alpha chain and beta chain to create a bicistronic expression vector. A signal sequence for secretion was included before the N-terminus of the alpha chain, and the Fos zipper was added to the C-terminus of the MHC-II alpha chain extracellular domain followed by an Avi tag (GLNDIFEAQKIEWHE) and a hexahistidine tag.[48,49] The class II-associated invariant chain peptide (CLIP) or a variant of CLIP was included before the N-terminus of the beta chain using a flexible glycine/serine linker. In some constructs, a thrombin or TEV protease cleavage site was included within the flexible linker between the CLIP peptide and the beta chain to facilitate peptide exchange. A signal sequence for secretion was included before the CLIP peptide, and the Jun zipper was added to the C-terminus of the beta chain extracellular domain followed by a hexahistidine tag.

Protein expression and purification

MHC-II proteins containing C-terminal Fos/Jun leucine zippers were expressed in Chinese Hamster Ovary (CHO) cells. Recombinant MHC-II was purified from cell culture supernatant by nickel-NTA chromatography using a HisTrap Excel column (Cytiva). Fractions containing pMHC-II were pooled and concentrated using a 10K MWCO Amicon centrifugal filter (Millipore Sigma, Cat#UFC901008).

The concentrated protein solution was then purified by size exclusion chromatography using a Superdex 200 10/300 GL column (Cytiva, Cat#28990944). Protein purity was determined to be >90% by SDS-PAGE.

Peptides for 2D-LCMS screening and tetramer generation

The peptides used for high-throughput 2D-LCMS screening were purchased from JPT at >70% purity, and the peptides used to prepare peptide-exchanged, biotinylated MHC-II monomers for tetramer generation were purchased from Elim Biopharma or GenScript at >95% purity. 4 mM stock solutions of each peptide were prepared in ethylene glycol and stored at −20°C.

Buffer exchange

pMHC-II was buffer exchanged into 25 mM Tris pH 8.0, 2 mM NaN_3 using a 2-mL 7K MWCO Zeba desalting column (Thermo Scientific™, Cat#89889) following the manufacturer's instructions and filtered using a 0.22 μm spin filter (EMD Millipore).

Thrombin cleavage

A 200 μL aliquot of thrombin-agarose (Sigma Cat# RECOMT-1KT) was washed with 4 mL of reaction buffer (25 mM Tris pH 8.0, 2 mM NaN_3) and centrifuged for 2 min at 1000 × *g*. The supernatant was discarded, and 4 mL of 1-5 mg/mL buffer-exchanged pMHCII was incubated with 200 μL of thrombin-agarose at room temp on a rotating mixer. The reaction progress was monitored by LCMS until cleavage was complete. The mixture was centrifuged at 1000 × *g* for 2 minutes to pellet the thrombin-agarose, and the supernatant was filtered through a 0.22 μm spin filter. The thrombin-agarose was washed with reaction buffer and stored in 25% glycerol, 12.5 mM Tris pH 8.0, 1 mM NaN_3 at 4°C.

TEV cleavage

1 mL of 2-5 mg/mL pMHC-II in PBS pH 7.4 was incubated at room temperature with 30 μg/mL of the TEV S219V variant.[50] The reaction progress was monitored by LCMS until cleavage was complete.

Biotinylation

In vitro biotinylation was performed using the *E. coli* biotin ligase BirA. Buffer-exchanged pMHC-II containing a C-terminal Avi tag was incubated at room temperature with BirA for at least two hours using the following reaction conditions: 10-50 μM pMHC-II-Avi-tag, 200 μM biotin, 10 mM magnesium acetate, 10 mM ATP, and 15 μg/mL BirA).

Purification of biotinylated pMHC-II

The reaction mixture was filtered using a 0.22 μm spin filter (EMD Millipore) and purified by size exclusion chromatography on a Superdex 200 10/300 GL column (Cytiva, Cat#28990944) equilibrated in PBS pH 7.4, 2 mM NaN_3. The sample was injected into the column and eluted at a flow rate of 0.5 mL/min. Fractions containing biotinylated pMHC-II were pooled, concentrated using a 10K MWCO Amicon centrifugal filter (Millipore Sigma, Cat#UFC901008), and filtered using a 0.22 μm spin filter. For short-term storage (1-2 months), the purified protein was stored at 4°C. For long-term storage, the protein was aliquoted into 0.2 mL PCR tubes, flash-frozen on dry ice, and stored at −80°C. The extent of biotinylation was confirmed by analytical size exclusion chromatography by mixing biotinylated pMHC-II at 1:1 and 2:1 ratio of pMHC-II-biotin to streptavidin-PE (BioLegend, Cat#405203).

Peptide exchange

A master mix of 17.8 μM protease-cleaved, biotinylated MHC-II was prepared in a buffer containing 44.5 mM sodium acetate pH 5.0, 167 mM NaCl, 4.45 mM Ethylenediaminetetraacetic acid (EDTA), and 2.23 mM NaN_3. For cysteine-containing peptides, 0.56 mM TCEP was added to the master mix to prevent disulfide formation. A 25-fold molar excess of peptide from a 4 mM stock solution in ethylene glycol was added to the MHC-II master mix to give a final composition of 16 μM MHC-II, 400 μM peptide, 40 mM sodium acetate pH 5, 150 mM NaCl, 4 mM EDTA, 2 mM NaN_3, and 0.50 mM TCEP. Peptide exchange was performed by incubating the mixture at 37°C for 60-72 hours. After incubation, an equal volume of 50 mM Tris pH 8.0, 150 mM NaCl was added to neutralize the mixture prior to 2D-LCMS analysis.

2D-LCMS

Two-dimensional liquid chromatography mass spectrometry (2D-LCMS) was used to evaluate the efficiency of *in vitro* peptide exchange with MHC-II proteins and peptides of interest following a previously published protocol.[32] In the first dimension, pMHC-II was separated on an analytical size exclusion column (Zenix SEC-100, 100 Å, 3 μm, 4.6 x 150 mm) from excess peptide in the reaction mixture and then collected in a sampling loop. In the second dimension, the purified pMHC-II collected in the sampling loop was injected into a reversed-phase column (Agilent PLRP-S, 1000 Å, 8 μm, 50 x 2.1 mm, Cat#PL1912-1802) to separate bound peptides from the MHC-II complex. 20 μL of approximately 0.5 mg/mL neutralized pMHC-II mixture were used for analysis. In the first dimension, the protein was eluted at 0.4 mL/min in 25 mM Tris pH 8.0, 150 mM NaCl, 2 mM NaN_3 for 11 min. In the second dimension, peptide(s) and MHC-II were separated using a gradient of 5–50% mobile phase B in 4.7 min at 0.55 mL/min with the column heated to 80°C [mobile phase A = 0.05% trifluoroacetic acid (TFA) in water, mobile phase B = 0.05% TFA in acetonitrile]. Eluted peptides and proteins from the second dimension were then sent to a mass spectrometer for electrospray ionization and mass detection in positive

ion mode (Agilent 6224 ESI-TOF LCMS). LCMS data analysis was performed using Agilent MassHunter Quantitative Analysis software. Combined extracted ion chromatograms (EICs) were prepared using the extracted intensities for the $[M+H]^{+}$, $[M+2H]^{2+}$, and $[M+3H]^{3+}$ ions. Query peptides with a combined EIC intensity of $>10^{3}$ were considered to be MHC-II binders.

LC-MS/MS identification of peptide impurity

Peptides were analyzed on an Agilent 6545XT AdvancedBio LC/Q-TOF Mass Spectrometer using an Agilent AdvanceBio Peptide Plus 2.7 μm column (2.1x150 mm, Cat#695775-949) equilibrated in 0.1% formic acid and developed with an acetonitrile gradient from 2% to 30% in 18 min at a flow rate of 0.25 mL/min. The column was heated to 50°C, and the column effluent was introduced into the mass spectrometer with JetSpray ionization. Peaks were subjected to CID (collision-induced dissociation) fragmentation as they eluted.

Tetramer generation

Tetramers were formed from fresh or frozen monomers. Frozen monomers (stored at -80°C) were thawed on ice. Fresh monomers were either prepared the day before or the same day of the staining. Both thawed or fresh monomers were combined to PE- or APC-streptavidin (BioLegend Cat#405207 (APC), Cat#405203 (PE) or Agilent Cat#PJRS25 (PE), Cat#PJ25S (APC)) after centrifugation (10,000 rpm for 10 min), and incubated for at least 20 min at 4°C. 10.26 μg of streptavidin was added to each 100 μg of monomers for a final concentration of 0.24 or 0.25 mg/mL of streptavidin-tetramers.

Immunogenicity assay

Immunogenicity was assessed by ELISpot and/or pI-A^{b} tetramer staining as specified in the results and legends. For ELISpot assays, 5 x 10^{5} CD8-depleted splenocytes (using the manufacturer's procedure with CD8a Ly2 microbeads (Miltenyi, Cat#130-117-044) and LS columns (Miltenyi, Cat#130-042-401) were cultured overnight at 37°C in RPMI containing 10% FBS (1% penicillin/streptomycin Gibco™ Cat#15140122, 1% HEPES Gibco™ Cat#15630130, 1% GlutaMAX Gibco™ Cat#35050061, 1% sodium pyruvate Gibco™ Cat#11360070) in a 96 well mouse IFN-gamma ELISpot plate (R&D Systems Cat#EL485). CD8-depleted splenocytes (containing APCs) were used to determine the $CD4^{+}$ T cell response in ELISpot assay (R&D Systems Cat#EL485), and only samples with less than 2% of $CD8^{+}$ T cells remaining after depletion were considered in the analysis. 24 mer peptide (25 μg/mL) or 13-16 mer MHC-II epitopes (2 μg/mL) were added into the culture, and cell stimulation was compared between mice immunized with neoantigen-specific vaccine (peptide/adjuvant or mRNA-LPX) and adjuvant alone or vehicle control after stimulation *in vitro* with the same concentrations of specific peptides. For analysis, IFN-gamma spots were counted using the manufacturer's procedure (R&D Systems Cat#EL485) and an automatic ELISpot reader (AID). All samples were tested with a minimum of 3 biological replicates in each individual experiment. Custom peptide synthesis was performed by either AnaSpec or GenScript ($\geq$ 75% purity).

Tetramer staining and flow cytometry

For MHC-II neoantigen-specific tetramer staining, 1-5 x 10^{6} splenocytes were washed with Hanks' Balanced Salt Solution (HBSS, Gibco™ Cat#14025092), and stained with PE- or APC- labeled pI-A^{b} tetramers in HBSS at 20 μg/mL for 1 hour at room temperature. Tetramer-positive cells were then enriched using the manufacturer's procedure for anti -PE or -APC microbeads (Miltenyi, Cat#130-048-801 and 130-090-855). Cells were then stained with a mix solution including the following antibodies and cell death stain in HBSS (Gibco™ Cat#14025092) for 20 min at 4°C: CD90.2 FITC (BD Biosciences, Cat#553004), CD4 APC-Cy7 (BD Biosciences, Cat#552051), CD8b PerCP-Cy5.5 (BD Biosciences, Cat#567597), CD44 AF700 (BioLegend, Cat#103026), I-A/I-E BV421 (BioLegend, Cat#107631), CD11b BV421 (BioLegend, Cat#101235), CD11c BV421 (BioLegend, Cat#117329), F4/80 BV421 (BioLegend, Cat#123131), TCRgd BV421 (BioLegend, Cat#118119), and Live Dead Blue (Live/Dead™ fixable blue dead cell stain kit, Invitrogen Cat#L23105). Cells were washed twice with MACS buffer (Genentech), filtered, and acquired on a BD Symphony flow cytometer. FlowJo software was used for analysis.

QUANTIFICATION AND STATISTICAL ANALYSIS

All data are presented as the mean ± standard deviation (SD). GraphPad Prism 10 was used for all analyses. The number of animals per experimental group is presented in each figure or in the relevant experimental sections above, and animals were randomly assigned to experimental groups.